Frequency-domain analytic method for efficient thermal simulation under curved trajectories laser heating

Daniel Mejia[a,b], Aitor Moreno[b], Jorge Posada[b], Oscar Ruiz-Salguero[a], Iñigo Barandiaran[b], Juan Carlos Poza[c], Raúl Chopitea[c]

[a]*Laboratorio de CAD CAM CAE, Universidad EAFIT, K49 #7 Sur-50, Medellín (Colombia)*
[b]*Vicomtech-IK4, Mikeletegi Pasealekua, 57, Donostia - San Sebastián (Spain)*
[c]*Lantek Investigación y Desarrollo, Parque Tecnológico de Alava - Ferdinand Zeppelin 2, 01510 Miñano, Álava (Spain)*

Abstract

In the context of Computer Simulation, the problem of heat transfer analysis of thin plate laser heating is relevant for downstream simulations of machining processes. Alternatives to address the problem include *(i)* numerical methods, which require unaffordable time and storage computing resources even for very small domains, *(ii)* analytical methods, which are less expensive but are limited to simple geometries, straight trajectories and do not account for material non-linearities or convective cooling. This manuscript presents a parallel efficient analytic method to determine, in a thin plate under convective cooling, the transient temperature field resulting from application of a laser spot following a curved trajectory. Convergence of both FEA (Finite Element Analysis) and the analytic approaches for a small planar plate is presented, estimating a maximum relative error for the analytic approach below 3.5% at the laser spot. Measured computing times evidence superior efficiency of the analytic approach w.r.t. FEA. A study case, with the analytic solution, for a large spatial and time domain ($1\,m \times 1\,m$ and $12\,s$ history, respectively) is presented. This case is not tractable with FEA, where domains larger than $0.05\,m \times 0.05\,m$ and $2\,s$ require high amounts of computing time and storage.

Keywords: Heat Transfer, Laser Heating, Analytic Solution, Efficient Simulation, Parallel Computing, Thin Plate

Email address: `amoreno@vicomtech.org` (Aitor Moreno)

Abbreviations

FEA	Finite Element Analysis.
a, b, Δz	Width (m), height (m) and thickness (m) of the plate.
$\mathbf{x}$, t	Spatial $\mathbf{x} = [x, y]$ ($[m, m]$) and temporal $t \geq 0$ (s) coordinates.
$u = u(\mathbf{x}, t)$	Temperature distribution along the plate at a given time (K).
ρ	Plate density (kg/m^3).
c_p	Plate specific heat ($J/(kg \cdot K)$).
k	Plate thermal conductivity ($W/(m \cdot K)$).
R	Plate reflectivity i.e., portion of the laser energy that is not absorbed by the plate ($0 \leq R \leq 1$).
$q = q(u)$	Heat loss due to convection at the thin plate surface (W/m^2).
h	Convection coefficient at the plate surface ($W/(m^2 \cdot K)$).
u_∞	Temperature of the plate surrounding medium (K).
$\mathbf{x}_0 = \mathbf{x}_0(t)$	Laser spot center location at a given time $[x_0(t), y_0(t)]$ ($[m, m]$).
$f = f(\mathbf{x}, \mathbf{x}_0)$	Laser power density model (W/m^2). There are four types in this manuscript: circle-shape (f_{circle}), square-shape (f_{square}), Gaussian ($f_{Gaussian}$) and Dirac delta (f_{Dirac}).
P	Laser power (W).
$\vec{v} = [v_x, v_y]$	Laser scanning speed (m/s).
r	Circle-shape laser spot radius (m).
Δx	Square-shape laser spot edge length (m).
σ	Parameter of the Gaussian laser model (m).
$\mathbb{X}_i = \mathbb{X}_i(x)$	i-th Fourier basis function in the x-axis.
$\mathbb{Y}_j = \mathbb{Y}_j(y)$	j-th Fourier basis function in the y-axis.
$\Theta_{ij} = \Theta_{ij}(t)$	ij-th Fourier coefficient for the temperature solution u.
$(\mathbf{\Omega}, \mathbf{X})$	Finite element discretization of the problem. $\mathbf{\Omega} = \{\Omega_1, \Omega_2, \ldots, \Omega_m\}$, $\mathbf{X} = \{\mathbf{x}_1, \mathbf{x_2}, \ldots, \mathbf{x}_n\}$.
Δt	Timestep size for the time discretization in FEA.
$\mathbf{U}^{(t)}$	Nodal values of the temperature for the FEA discretization of the problem. $\mathbf{U}^{(t)} = [u(\mathbf{x}_1, t), u(\mathbf{x}_2, t), \ldots, u(\mathbf{x}_n, t)]^T$.
$\mathbf{F}^{(t)}$	Nodal values of the laser source for the FEA discretization of the problem. $\mathbf{F}^{(t)} = [f(\mathbf{x}_1, t), f(\mathbf{x}_2, t), \ldots, f(\mathbf{x}_n, t)]^T$.

1. Introduction

Thin plate laser heating is an important manufacturing process in which a high powered laser source (such as a CO_2 or Nd-YAG laser) is applied to locally heat, melt and/or remove the plate material. Applications include metal plate alloying, drilling, forming, bending and cutting.

Numerical computer simulations of laser applications consume large computing resources, even for very small domains. On the other hand, analytic or closed form formulations require much less computer resources, at the price of lower precision and significant restrictions on the application circumstances. However, these analytic solutions become appealing as they may produce economic forecasts of the overall heating process, for specific study cases.

This manuscript presents an efficient analytic solution for the time history of the temperature field of thin rectangular flat plates heated by a constant speed laser spot. Unlike other analytic methods, our solution considers convective energy exchange and piecewise linear curved trajectories. It handles time and space domains sizes significantly larger than the feasible for FEA. Our method uses Fourier coefficients to find a solution in the frequency domain and maps it back to the time-space domain. We compute the solution for timestep t_n and trajectory piece $\mathbf{x_0}(t_n)$ based on timestep t_{n-1} and trajectory piece $\mathbf{x_0}(t_{n-1})$. The presented algorithm enables easy parallelization resulting in further improvement in the overall efficiency for larger space and/or time domains

This article is organized as follows: Sect. 2 reviews the relevant literature. Sect. 3 describes the methodology. Sect. 4 presents and discusses results of the conducted experiments. Sect. 5 concludes the paper and introduces what remains for future work.

2. Literature review

This section discusses the state of the art for the simulation of the laser heating problem. Sect. 2.1 reviews the literature concerning numerical approaches to the problem solution while Sect. 2.2 discusses the analytic approaches. Sect. 2.3 concludes the literature review.

2.1. Numerical methods for laser heating simulation

FEA is one of the most important numerical tool for thermodynamic analysis of metal plates under laser heating. Yan et al. [1], Joshi et al. [2]

perform a parametric study on a rectangular plate using FEA in order to measure the impact of laser speed, laser spot radius and laser power on the plate temperature distribution during laser heating. Hagenah et al. [3] performs and statistically validates the parametric analysis using ANOVA tests. Yilbas and Akhtar [4], Yilbas et al. [5] solve a thermal/stress model with FEA in order to study the plate deformations due to the high temperature gradients. Kadri et al. [6] compare FEA with trained ANN (Artificial Neural Networks) for predicting thermal stresses in laser cutting of glass sheets.

Akhtar et al. [7], Yilbas et al. [8] simulate rectangular cuts with laser using FEA, while Akhtar [9], Yilbas et al. [10] perform the same analysis for circular and triangular cuts respectively. The enthalpy method is used to account for non-linearites of the material as well as phase changes that induce material melting. Experimental validation of the estimated temperature is presented using thermocouples.

Roberts et al. [11] investigate the laser heating problem using the element birth and death method in order to account for material non-linearities. For accounting material removal in the FEA models, Akarapu et al. [12], Nyon et al. [13], Fu et al. [14] incorporate a temperature-threshold approach which removes melted elements from the plate mesh during the simulation.

Aside from FEA, other numerical methods have been used for simulation of laser heating processes. Modest [15, 16], Han and Na [17], Xu et al. [18] use the Finite Differences Method (FDM) for the analysis of laser heating phenomenon while Kim [19, 20] employs a Boundary Element Method (BEM) approach. Recently, the Finite Volume Method (FVM) has been incorporated for the simulation of the laser heating problem [21, 22].

Despite the modeling complexity that can be reached with numerical tools, these approaches are highly sensitive to spatial and time discretizations of the plate [23, 24, 25]. Therefore, such approaches are currently unusable in industrial scenarios where fast decisions must be made for large plates and complex laser trajectories.

2.2. Analytic methods for laser heating simulation

Analytic (or semi-analytic) solutions to the problem have been also proposed in the literature of laser heating simulation. Modest and Abakians [26] develop an ordinary non-linear differential equation which is then solved numerically for the laser heating problem. Zimmer [27] solves a 1D laser heating problem for solid-liquid interfaces using the Laplace transform. Mullick et al. [28] develop a non-linear analytic model which is solved iteratively to estimate the plate temperature in underwater laser cutting. The model is then validated numerically and statistically [29]. Jiang and Dai [30] present an analytic solution for the thermal/stress equations by means of Fourier series. Winczek [31] presents an analytic solution for the 3D laser heating problem for piecewise linear trajectories by a superposition of fundamental solutions in a semi-infinite domain. Convective heat losses are omitted at the plate surface and the plate is assumed with infinite depth.

Analytic approaches provide computationally faster results than numerical approaches. However, they are very limited in model assumptions [32]. Such limitations include: linear laser trajectories, 1D and 2D rectangular domains, constant material properties and null convection on the plate surface.

2.3. Conclusions of the literature review

As discussed above, numerical tools are impractical for industrial scenarios [24, 25] where decisions must be made on large plate sizes. Current analytic approaches partially overcome this problem by providing fast solutions at the cost of limitations such linear trajectories, no convection at the plate surface and material properties independent of the temperature. However, they only work for linear trajectories on the plate.

This manuscript presents an analytic solution for the 2D laser heating of rectangular thin plates problem. Our algorithm: *(1)* acts recursively in the time domain calculating the Fourier solution for time t_n using the coefficients from timestep t_{n-1}, *(2)* allows parallelization for computing the Fourier coefficients of timestep t_n. Features *(1)* and *(2)* are the basis for the algorithm low computational cost. Our analytic approach covers larger space and time domains than the ones achieved by FEA methods. A study case is presented in order to compare the convergence rate and execution times of the algorithm vs. FEA in a MATLAB implementation.

To illustrate the capabilities of the implemented approach, a study case for a large plate ($1\,m^2$, $12\,s$ history) is presented. Table 1 presents an appraisal of this manuscript contributions versus other approaches in the current literature.

3. Methodology

This section discusses the methodology for our analytic solution to the laser heating problem and poses a study case. Sect. 3.1 introduces the theoretical model and assumptions for the heat transfer analysis. Sect. 3.2

Ref.	Curved Laser Trajectory	Convection at the Surface	Nonlinear Thermal Properties	Large Domain Study
Our Analytic Method	Yes	Yes	No	Yes
[26]	No	No	No	No
[27]	No	No	No	No
[28]	No	Yes	Yes	No
[30]	No	No	No	No
[31]	Yes	No	No	Yes
FDM [18]	No	Yes	No	No
BEM [20]	No	Yes	No	No
FEA [5]	Yes	Yes	Yes	No
FVM [22]	No	Yes	Yes	No

Table 1: Comparison of the contributions and drawbacks of our analytic method and some state of the art methodologies.

presents the analytic solution to the problem. Sect. 3.3 discusses about the different laser models. Sect. 3.4 describes the implementation details of the solution. Sect. 3.5 briefly discusses the FEA approach used to validate numerically the analytic solution. Finally, Sect. 3.6 presents a simulation case of study.

3.1. Heat equation for the thin plate laser heating problem

In the case of metal plates, it is reasonable to ignore heat transfer through the plate thickness (i.e. using a 2D model $\nabla \cdot k\nabla = k\frac{\partial^2}{\partial x^2} + k\frac{\partial^2}{\partial y^2}$) due to the relative size of the plate thickness w.r.t. its width and height ($\Delta z \to 0$) and the high thermal conductivity. According to Ref. [33], heat transfer in a 2D plate subject to a continuous laser source satisfies the following PDE with initial and boundary conditions:

$$\begin{aligned} \rho c_p \frac{\partial u}{\partial t} - \nabla \cdot (k \nabla u) &= \frac{f - q}{\Delta z} \\ q &= h(u - u_\infty) \\ u|_{x=0} = u|_{x=a} &= u|_{y=0} = u|_{y=b} = u_\infty \\ u(\mathbf{x}, 0) &= u_\infty \end{aligned} \tag{1}$$

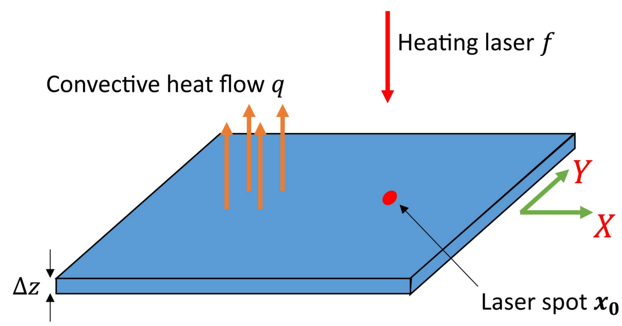

Figure 1: Schematic of the laser heating model. A laser passes an amount of energy f at a plate location $\mathbf{x_0}$ while the plate cools down due to convection q at the surface.

where ρ, c_p and k are the material density, specific heat and thermal conductivity respectively (assumed constant in this manuscript). u is the temperature distribution on the plate. f is the laser surface power density of the laser (discussed in Sect. 3.3) and q is the heat loss due to convection at the plate surface. The plate initial temperature is assumed at constant ambient temperature u_∞ and the 2D borders of the plate are assumed at ambient temperature for the whole simulation. An scheme of the laser heating problem is depicted in Fig. 1.

3.2. Analytic solution of the problem

Following the same procedure as in [30], the following analytic solution for the temperature distribution can be derived for Eq. (1):

$$u(\mathbf{x}, t) = u_\infty + \sum_{i=1}^{\infty} \sum_{j=1}^{\infty} \Theta_{ij}(t) \mathbb{X}_i(x) \mathbb{Y}_j(y) \tag{2}$$

with Fourier basis functions:

$$\begin{aligned} \mathbb{X}_i(x) &= \sin \frac{i\pi x}{a} \\ \mathbb{Y}_j(y) &= \sin \frac{j\pi y}{b} \end{aligned} \tag{3}$$

and their respective Fourier coefficients $\Theta_{ij}(t)$. The value for these coefficients is given below.

3.2.1. Fourier Coefficients

The closed form of the Fourier coefficients $\Theta_{ij}(t)$ from Eq. (2) can be derived using separation of variables [30]:

$$\Theta_{ij}(t) = \frac{4}{ab\rho c_p \Delta z} \int_{t_0}^{t} \int_0^b \int_0^a f(\mathbf{x}, \mathbf{x}_0(\tau)) \mathbb{X}_i(x) \mathbb{Y}_i(y) e^{-\omega_{ij}(t-\tau)} dx dy d\tau \tag{4}$$

where ω_{ij} are the eigenvalues of Eq. (3) for the current operator (Eq. (1)) defined as:

$$\omega_{ij} = \frac{k}{\rho c_p} \left(\frac{i^2\pi^2}{a^2} + \frac{j^2\pi^2}{b^2} \right) + \frac{h}{\rho c_p \Delta z} \tag{5}$$

The curved trajectory $\mathbf{x_0}(t)$ is discretized into a sequence of linear trajectories $\mathbf{x_0}(t) = [\mathbf{x}_0(t_0), \mathbf{x}_0(t_1), \cdots, \mathbf{x}_0(t_n)]$. Therefore, Eq. (4) becomes:

$$\begin{aligned} \Theta_{ij}(t_n) = \frac{4}{ab\rho c_p \Delta z} \sum_{l=0}^{n} e^{-\omega_{ij}(t_n - t_l)} \\ \int_{t_l - 1}^{t_l} \int_0^b \int_0^a f(\mathbf{x}, \mathbf{x}_0(\tau)) \mathbb{X}_i(x) \mathbb{Y}_i(y) e^{-\omega_{ij}(t_l-\tau)} dx dy d\tau \end{aligned} \tag{6}$$

Such discretization allows to compute easier the integral term in Eq. (4) for the nonlinear laser trajectory as a sum of linear laser trajectories.

3.2.2. Recursive Fourier Coefficients

Eq. (6) can be rewritten in recursive form as follows:

$$\begin{aligned} \Theta_{ij}(t_n) =& \Theta_{ij}(t_{n-1}) e^{-\omega_{ij}(t_n - t_{n-1})} + \\ & \frac{4}{ab\rho c_p \Delta z} \int_{t_{n-1}}^{t_n} \int_0^b \int_0^a f(\mathbf{x}, \mathbf{x}_0(\tau)) \mathbb{X}_i(x) \mathbb{Y}_i(y) e^{-\omega_{ij}(t_n-\tau)} dx dy d\tau \end{aligned} \tag{7}$$

where $\Theta_{ij}(t_{n-1})$ are the Fourier coefficients of a previous timestep solution (recursive term). In the time domain, the term $\Theta_{ij}(t_n)$, for time t_n can be economically solved in recursive manner by using the term $\Theta_{ij}(t_{n-1})$ instead of computing the whole history. Furthermore, since the laser trajectory has been discretized into linear paths, the integral term in Eq. (7) accounts for a linear laser trajectory at time t_n. Therefore, such integral can be solved easier than using a nonlinear path.

3.3. Laser source models

Eq. (7) requires evaluating the following integral for the laser beam source:

$$\int_{t_{n-1}}^{t_n}\int_0^b\int_0^a f(\mathbf{x},\mathbf{x}_0)\mathbb{X}_i(x)\mathbb{Y}_j(y)e^{-\omega_{ij}(t_n-\tau)}dxdyd\tau \tag{8}$$

The value of such integral depends on the laser model used. The most common models used are: circle-shape laser model (f_{circle}, Fig. 2(a)), square-shape laser model (f_{square}, Fig. 2(b)), Gaussian laser model ($f_{Gaussian}$, Fig. 2(c)) and Dirac delta laser model (f_{Dirac}). Each of these models are presented below:

$$\begin{aligned}
f_{circle}(\mathbf{x},\mathbf{x_0}) &= \begin{cases} \frac{P(1-R)}{\pi r^2}, & \|\mathbf{x}-\mathbf{x}_0\| < r \\ 0, & otherwise \end{cases} \\
f_{square}(\mathbf{x},\mathbf{x_0}) &= \begin{cases} \frac{P(1-R)}{\Delta x^2}, & |x-x_0| < \frac{\Delta x}{2} \quad and \\ & |y-y_0| < \frac{\Delta x}{2} \\ 0, & otherwise \end{cases} \\
f_{Gaussian}(\mathbf{x},\mathbf{x_0}) &= \frac{P(1-R)}{\pi\sigma^2}e^{\left(-\frac{\|\mathbf{x}-\mathbf{x}_0\|^2}{\sigma^2}\right)} \\
f_{Dirac}(\mathbf{x},\mathbf{x_0}) &= \lim_{\sigma\to 0} f_{Gaussian}(\mathbf{x},\mathbf{x_0})
\end{aligned} \tag{9}$$

Solution for Eq. (8) is presented in the Appendix for an f_{square} laser source and an f_{Dirac} laser source. For the other two laser models, Table 2 presents an equivalence between laser parameters such that the overall input energy $\int_0^b\int_0^a f(\mathbf{x},\mathbf{x_0})dxdy$ and the power density peak $\max_{\mathbf{x}} f(\mathbf{x},\mathbf{x_0})$ of the laser beam are the same independently of the model. As the laser spot becomes smaller, all the energy input localizes in a smaller area despite the chosen model as illustrated in Fig. 3. Therefore, for relatively small laser spots (w.r.t. the 2D plate size), the heat transfer phenomenon described in Eq. (1) should behave similarly for all the laser models.

3.4. Algorithm overview

To apply the analytic solution posed in Eq. (2), the curved laser trajectory $\mathbf{x}_0(t)$ is discretized into a sequence of linear trajectories $\mathbf{x_0}(t) = [\mathbf{x}_0(t_0), \mathbf{x}_0(t_1), \cdots, \mathbf{x}_0(t_n)]$. Such discretization is achieved by uniformly sampling the parametric trajectory such that the timestep remains constant through the whole simulation. Afterwards, Eq. (7) is applied recursively

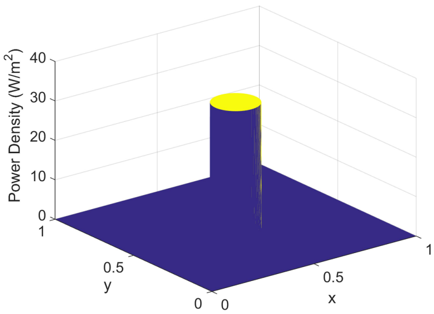

(a) Circle-shape laser beam model f_{circle} distribution.

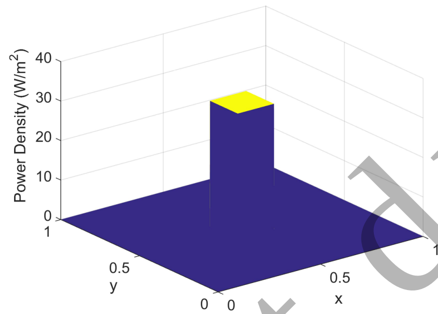

(b) Square-shape laser beam model f_{square} distribution.

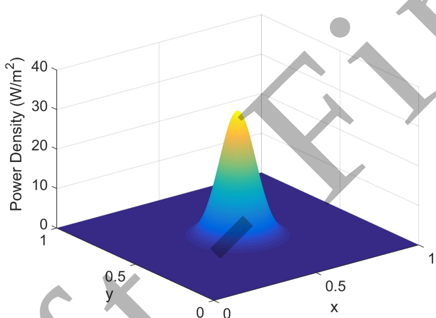

(c) Gaussian laser beam model $f_{Gaussian}$ distribution.

Figure 2: Laser model distribution for the different laser beam models: f_{circle}, f_{square} and $f_{Gaussian}$.

Model	Parameter	Value
Circle-shape	r	
Square-shape	Δx	$\Delta x = r\sqrt{\pi}$
Gaussian model	σ	$\sigma = r$
Dirac laser		$r \to 0$

Table 2: Equivalence table between laser model parameters.

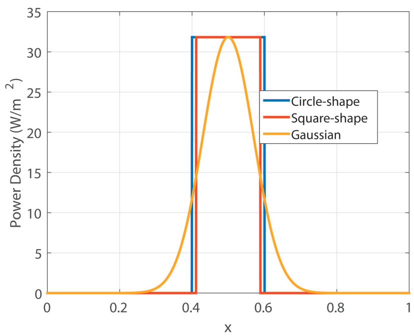

(a) Laser power density distribution for a spot radius $r = a/10$.

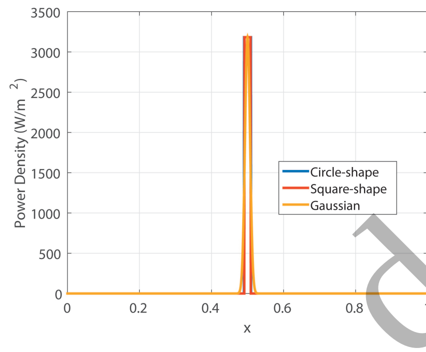

(b) Laser power density distribution for a spot radius $r = a/100$.

Figure 3: Distribution of the laser power densities for the different laser models along the x-axis using different laser spot sizes.

on the sequence of linear trajectories in order to compute the Fourier coefficients at each timestep. Since $u(\mathbf{x}, t_0) = u_\infty$, the algorithm is initialized by setting $\Theta_{ij}(t_0) = 0$. Finally, the temperature solution $u(\mathbf{x}, t_l)$ at any timestep t_l can be recovered by applying Eq. (2). The infinite sum is truncated in order to obtain an approximate solution. Fig. 4 presents an overview of the algorithm.

3.5. Numerical Comparison with FEA

In order to validate numerically the implemented approach, FEA is used to simulate the laser heating problem. The FEA linear system of equations that arises for Eq. (1) is:

$$\left[\left(\frac{\rho c_p}{\Delta t} + \frac{h}{\Delta z}\right)\mathbf{M} + k\mathbf{L}\right]\mathbf{U}^{(t+\Delta t)} = \mathbf{M}\left(\frac{\rho c_p}{\Delta t}\mathbf{U}^{(t)} + \frac{1}{\Delta z}\int_t^{t+\Delta t}\mathbf{F}^{(\tau)}\mathrm{d}\tau + \frac{h}{\Delta z}u_\infty\right) \tag{10}$$

where:

$$\begin{aligned} \mathbf{L}_{ij} &= \sum_{\Omega_k \in \mathbf{\Omega}} \int_{\Omega_k} \nabla\phi_i \cdot \nabla\phi_j \mathrm{dA} \\ \mathbf{M}_{ij} &= \sum_{\Omega_k \in \mathbf{\Omega}} \int_{\Omega_k} \phi_i\phi_j \mathrm{dA} \end{aligned} \tag{11}$$

are the Laplace-Beltrami (stiffness) and norm (mass) matrices respectively. $\mathbf{\Omega} = \{\Omega_1, \Omega_2, \ldots, \Omega_m\}$, $\mathbf{X} = \{\mathbf{x}_1, \mathbf{x_2}, \ldots, \mathbf{x}_n\}$ is a discretization of the plate

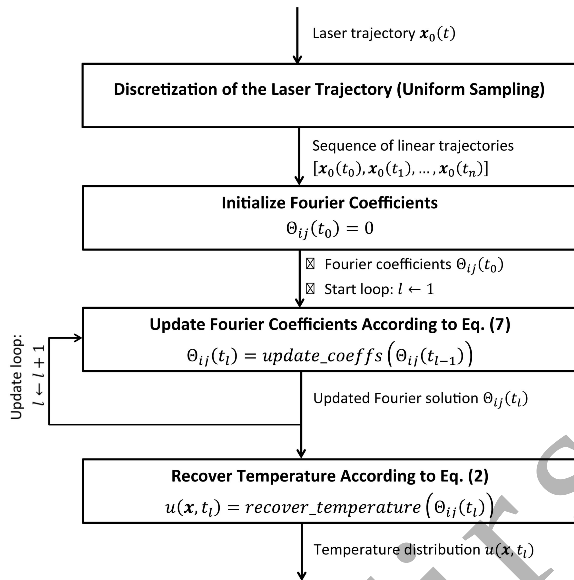

Figure 4: Diagram of the analytic approach algorithm.

into finite elements. $\phi_i = \phi_i(\mathbf{x})$ is the interpolation function associated to the node $\mathbf{x}_i$. $\mathbf{U}^{(t)} = [u(\mathbf{x}_1, t), u(\mathbf{x}_2, t), \dots, u(\mathbf{x}_n, t)]^T$ and $\mathbf{F}^{(t)} = [f(\mathbf{x}_1, t), f(\mathbf{x}_2, t), \dots, f(\mathbf{x}_n, t)]^T$ are the nodal values of the temperature and the laser source respectively. Finally, Δt is the timestep size.

To carry out the comparison of our analytic algorithm with FEA, a small study case (which can be solved accurately with FEA) is simulated with both approaches: a $0.01\,m \times 0.01\,m \times 0.001\,m$ AISI 304 steel plate (Table 3) is heated by a $P = 100\,W$, $r = 0.0003\,m$ squared laser source (f_{square}) which follows the trajectory depicted in Fig. 5 at constant speed $\|\vec{v}\| = 0.1\,m/s$. To discretize the plate, triangular elements are used with linear interpolation (Fig. 6). A timestep $\Delta t = 0.0012\,s$ is chosen for the time discretization.

3.6. Experimental setup

To test the implemented algorithm, a simulation study case with a relatively large plate is presented (computationally impractical for FEA). A $1\,m \times 1\,m \times 0.001\,m$ AISI 304 steel plate (Table 3) is heated by a $P = 100\,W$ point laser source (f_{Dirac}) that follows the trajectory depicted in Fig. 5 at constant speed $\|\vec{v}\| = 0.1\,m/s$. The surface of the plate is surrounded by air, which cools the plate by natural convection. Ambient temperature is set at

Parameter	Value
ρ	$8030\,kg/m^3$
c_p	$574\,J/(kg \cdot K)$
k	$20\,W/(m \cdot K)$
R	0
h	$20\,W/(m^2 \cdot K)$
u_∞	$300\,K$

Table 3: Physical parameters for simulation of laser heating of an AISI 304 steel plate (Ref. [4]). Natural convection due to surrounding air is considered.

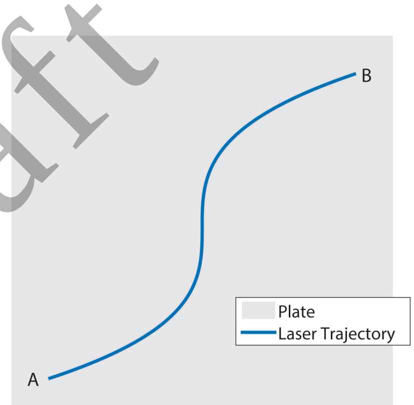

Figure 5: Trajectory of the laser on the plate surface (from A to B).

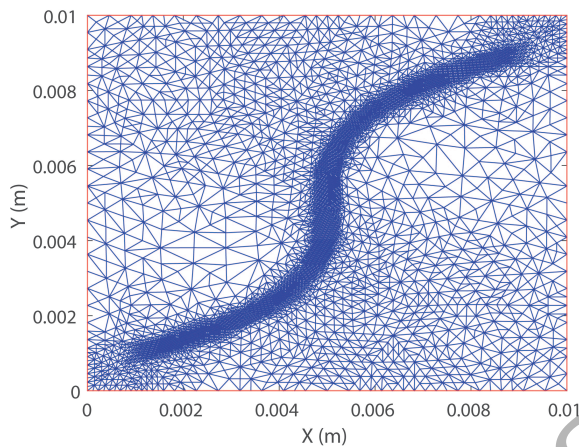

Figure 6: Triangular mesh discretization of the plate for FEA.

300 K.

4. Results and discussion

This section presents and discusses a numerical comparison of the implemented analytic method against FEA for a small plate study case (Sect. 4.1). Sect. 4.2 presents results of our analytic algorithm for a large plate study case, where current FEA becomes impractical computationally. Finally, Sect. 4.3 compares measured execution times for the analytic (serial and parallel implementation) and FEM approaches.

4.1. Numerical comparison of the analytic solution vs. FEA

This section presents the numerical results of the study case presented and discussed in Sect. 3.5. These results are used to compare the analytic approach with FEA. Fig. 7(a) plots the plate temperature distribution at the end of the simulation ($t = 0.12\,s$) estimated with our analytic approach. For this particular case, Eq. 2 is truncated at 200×200 Fourier terms since: *(1)* the error of the solution does not change significantly with more Fourier terms, and *(2)* such error is tolerable (below 3.5%). Fig. 7(b) plots the FEA temperature at the same simulation time. A timestep of $\Delta t = 0.0012\,s$ is used and the triangular mesh in Fig. 6 is for both FEA and our analytic solution (as per Eq. (2)). Fig. 7(c) plots the relative error distribution

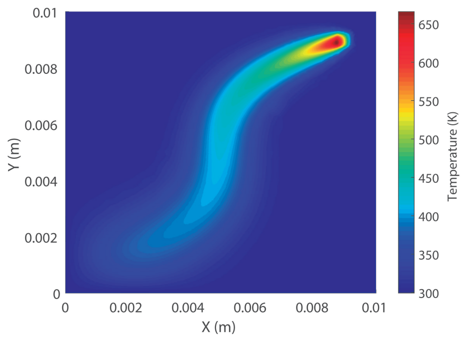

(a) Analytic temperature distribution at $t = 0.12\,s$.

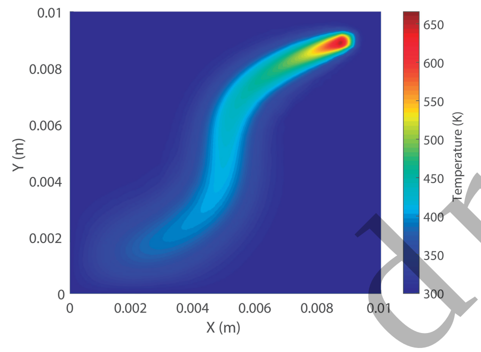

(b) FEA temperature distribution at $t = 0.12\,s$.

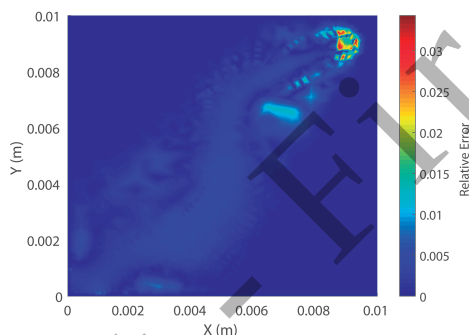

(c) Relative error of the analytic solution vs. FEA. The maximum relative error is 3.43%.

Figure 7: Temperature and error distribution for a small plate ($0.01\,m \times 0.01\,m \times 0.001\,m$) obtained by the analytic and FEA approaches.

of the analytic temperature considering the FEA solution as reference. A maximum relative error of 3.43% is measured around the laser spot.

Fig. 8(a) plots the maximum relative error of the analytic solution as a function of the number of Fourier terms in Eq. (2). The analytic solution stabilizes above 100×100 Fourier terms for the current study case (a relative error of $\approx 3.5\%$). Fig. 8(b) shows, in contrast, that the FEA solution falls below a relative error of 2% for mesh sizes above 10000 nodes. A FEA solution with a high resolution mesh ($> 50K$ mesh nodes) is used as reference temperature in both cases (MATLAB adaptive remeshing used). This relative analysis is only applicable to the described study case, as the

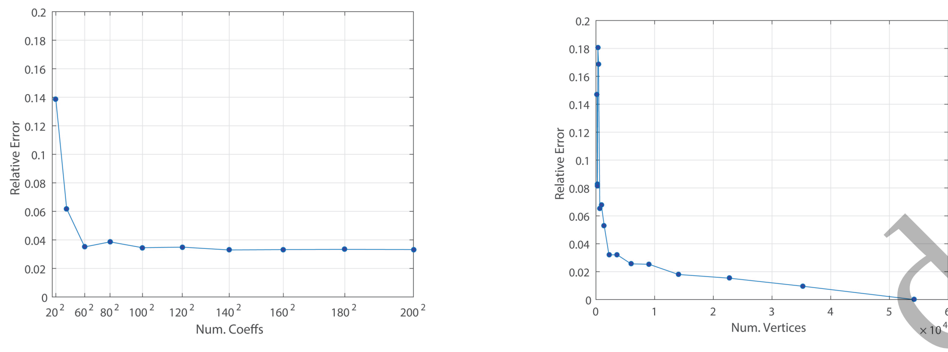

(a) Error of our analytic solution as a function of the number of Fourier terms.

(b) Error in the FEA solution as a function of the number of nodes.

Figure 8: Maximum relative error evolution for the analytic and FEA methods for the study case in Sect. 3.5 (the reference solution is a $54K$ node FEA simulation).

convergence of the problem is dependent on the laser spot radius / plate size ratio. Larger plates (or smaller laser spots) require more Fourier terms in the analytic case and larger meshes in the FEA case in order to accurately simulate the physical phenomenon.

4.2. Experiment results

This section presents the results obtained the analytic approach for the large study case ($1\,m \times 1\,m \times 0.001\,m$) in Sect. 3.6. A point source f_{Dirac} is used to simulate the laser. The Fourier series is set to 2000×2000 terms. Fig. 9 presents the evolution of the temperature field on the plate at different simulation times. Figs. 9(a) and 9(b) plot the temperature at early ($t = 0.6189\,s$) and halfway ($t = 6.1892\,s$) stages respectively while Fig. 9(c) plots the temperature at the end of the laser trajectory ($t = 12.3786\,s$). The zoom near the laser spot exhibits the high spatial resolution captured by our analytic solution.

4.3. Computing times

This section compares the analytic vs. FEA computing times for the case in Sect. 3.5. In the FEA case, Eq. (10) is implemented in MATLAB and solved using a linear solver for sparse matrices (sparse Cholesky factorization library `CHOLMOD`).

Our analytic solution lends itself for parallel computing. Our algorithm in Sect. 3.4 requires computing each Fourier coefficient $\Theta_{ij}(t)$ (Eq. (7)) as

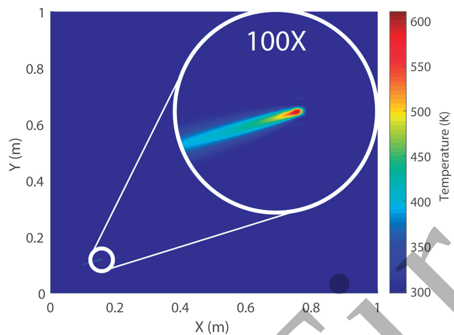

(a) Plate temperature distribution at $t = 0.6189\,s$.

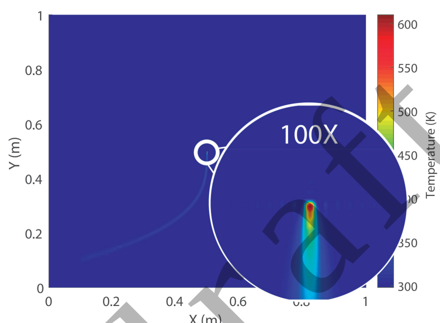

(b) Plate temperature distribution at $t = 6.1892\,s$.

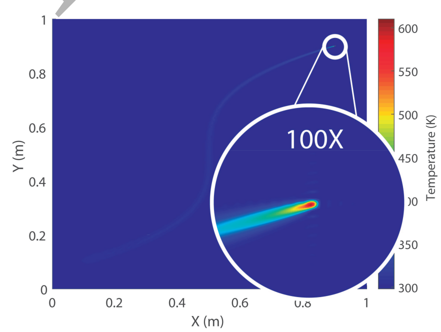

(c) Plate temperature distribution at $t = 12.3783\,s$.

Figure 9: Simulated temperature distribution for the large plate ($1\,m \times 1\,m \times 0.001\,m$) case study at different timestamps.

Item	Specifications
Operating System	Microsoft Windows 10 Home Single Language
Processor	Intel©Core™i7-4700HQ CPU @2.40GHz 2394 Mhz
Random Access Memory (RAM)	16.0 GB
Operating System Type	64 bits (x64)
GPU Unit	NVIDIA GeForce GTX 760M
Software	MATLAB R2014b 64-bit (win64), MATLAB Parallel Computing Toolbox

Table 4: Hardware and software specifications of the machine used to run FEA and the analytic simulations in both serial and parallel form.

a sequence of simple operations (such as sums, products and powers) independent from each other. These sequences of operations are independent between Fourier coefficients. In addition, the temperature field from Eq. (2) describes the temperature at each point $\mathbf{x}$ in the domain as a linear combination of the Fourier basis. Hence, the temperature can be recovered for each point $\mathbf{x}$ in the domain independently of others points. Therefore, we implement the analytic algorithm using both MATLAB basic operations (serial implementation) as well as `gpuArray` operations from the MATLAB Parallel Computing Toolbox (parallel implementation). Table 4 lists the software and hardware specifications of the machine used to run FEA, as well as the analytic algorithm in both serial and parallel form. Such configuration is a low end for numerical computing. This modest demand poses an advantage for our analytic approach.

Fig. 10 plots the measured execution times for computing the Fourier coefficients (Eq. (7)) with the analytic approach as a function of the number of Fourier terms in both serial and parallel implementations for the small plate case. The temperature recovery step of Eq. (2) is not included in the measured times. The intersection point between the serial and parallel times in the plot is near the 60×60 Fourier coefficients and the the gap between the serial and parallel execution times becomes larger as the number of Fourier coefficients increases. Therefore, the parallel version of the algorithm becomes in fact, significantly faster than the serial one for larger number of coefficients.

Fig. 11 presents the execution times for FEA and the serial analytic algo-

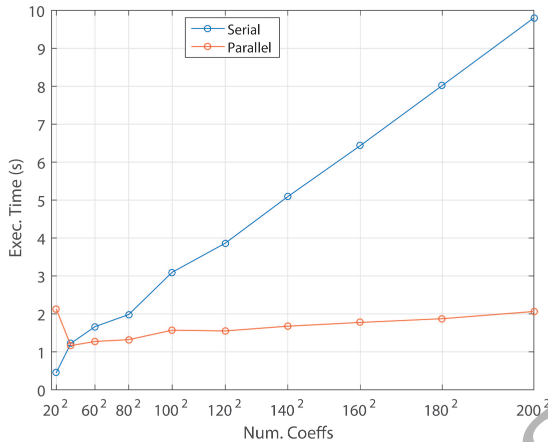

Figure 10: Serial and parallel execution times for computing the analytic Fourier solution (Eq. (7)) vs. number of Fourier coefficients used for the small plate case study (Sect. 3.5). The temperature recovery step of Eq. (2) is not considered.

rithm as a function of the number of mesh nodes and the number of Fourier terms (for the analytic case). The measured computation times consider the computation of the Fourier terms at each timestep and the recovery of the temperature (as per Eq. (2)) at the end of the simulation in the case of the analytic approach. However, the meshing step is not taken into account for measuring analytic or FEA times. Our analytic approach performs significantly faster than FEA as the mesh size increases, even for a large number of Fourier coefficients. Such difference in efficiency becomes crucial as the problem grows to bigger domains where FEA becomes very expensive computationally. For simplicity of the plot, parallel times are not included in Fig. 11. However, our experiments showed that the parallel implementation of the analytic algorithm performs better than the serial one (and therefore, better than FEA).

5. Conclusions and future work

This paper has presented a parallel efficient analytic solution for the 2D rectangular plate laser heating problem for curved laser trajectories and convection at the plate surface. Our algorithm discretizes the curved laser trajectory as a piecewise linear trajectory with constant speed. The solution for timestep t_n in the trajectory $\mathbf{x_0}(t_n)$ uses the result accumulated till the previ-

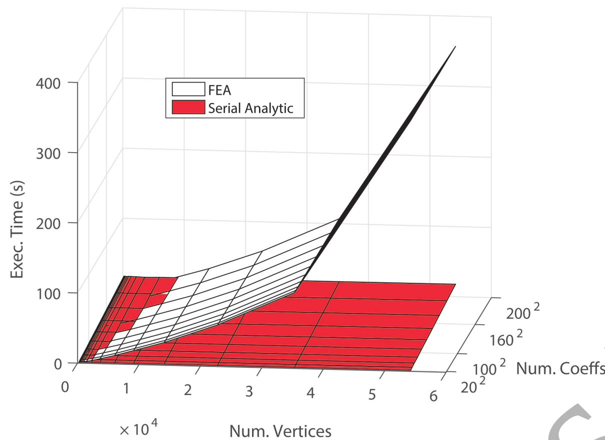

Figure 11: Execution times for computing the temperature solution with FEA and the serial analytic approaches w.r.t. the mesh size and the number of Fourier coefficients used in the analytic approach. Both Fourier computation times (Eq. (7)) and temperature recovery times (Eq. (2)) are considered. Meshing times are not considered.

ous timestep t_{n-1}. Our analytic solution allows to consider convective energy into the balance. Although the assumptions of the mathematical model simplify the laser heating phenomenon (constant material properties, no phase changes and constrained plate and laser geometries), the analytic algorithm provides an efficient solution to problems that are very expensive computationally for current FEA methods. Computing times of our algorithm are significantly lower than the FEA times for the same problem. Numerical comparison of the analytic method with FEA presents a relative error that reaches a maximum of 3.5% in very localized areas at the laser spot. Results for a $1\,m \times 1\,m \times 0.001\,m$ AISI 304 steel plate during $12.37\,s$ history (intractable with FEA) are presented for our analytic method.

Ongoing investigation includes: *(1)* assessment in industrial environments, *(2)* influence of nonconstant material properties, and *(3)* material melting and evaporation.

Acknowledgements

This work was supported by the EAFIT University, Vicomtech-IK4, Lantek Business Solutions and the Basque Government under the GAITEK and HAZITEK programs.

References

[1] Y. Yan, L. Ji, Y. Bao, X. Chen, Y. Jiang, CO2 laser high-speed crack-free cutting of thick-section alumina based on close-piercing lapping technique, Int. J. Adv. Manuf. Tech. 64 (9) (2012) 1611 – 1624, ISSN 1433-3015, doi:10.1007/s00170-012-4127-y.

[2] A. Joshi, N. Kansara, S. Das, P. Kuppan, K. Venkatesan, A Study of Temperature Distribution for Laser Assisted Machining of Ti-6Al-4 V Alloy, Procedia Engineering 97 (2014) 1466 – 1473, ISSN 1877-7058, doi:10.1016/j.proeng.2014.12.430, 12th Global Congress on Manufacturing and Management GCMM - 2014.

[3] H. Hagenah, M. Geiger, M. Merklein, Numerical simulation to improve robustness in sheet metal forming process chains, AIP Conf. Proc. 1532 (1) (2013) 683 – 688, doi:10.1063/1.4806895.

[4] B. Yilbas, S. Akhtar, Laser bending of metal sheet and thermal stress analysis, Opt. Laser Technol. 61 (2014) 34 – 44, ISSN 0030-3992, doi:10.1016/j.optlastec.2013.12.023.

[5] B. Yilbas, S. Akhtar, C. Karatas, H. Ali, K. Boran, M. Khaled, N. Al-Aqeeli, A. Aleem, Laser treatment of aluminum composite and investigation of thermal stress field, Int. J. Adv. Manuf. Tech. (2016) 1 – 15ISSN 1433-3015, doi:10.1007/s00170-015-8202-z.

[6] M. Kadri, S. Nisar, S. Khan, W. Khan, Comparison of ANN and finite element model for the prediction of thermal stresses in diode laser cutting of float glass, Optik - International Journal for Light and Electron Optics 126 (19) (2015) 1959 – 1964, ISSN 0030-4026, doi:10.1016/j.ijleo.2015.05.033.

[7] S. Akhtar, O. Kardas, O. Keles, B. Yilbas, Laser cutting of rectangular geometry into aluminum alloy: Effect of cut sizes on thermal stress field, Opt. Laser Eng. 61 (2014) 57 – 66, ISSN 0143-8166, doi:10.1016/j.optlaseng.2014.04.016.

[8] B. Yilbas, S. Akhtar, C. Karatas, Laser cutting of rectangular geometry into alumina tiles, Opt. Laser Eng. 55 (2014) 35 – 43, ISSN 0143-8166, doi:10.1016/j.optlaseng.2013.10.006.

[9] S. Akhtar, Laser cutting of thick-section circular blanks: thermal stress prediction and microstructural analysis, Int. J. Adv. Manuf. Tech. 71 (5) (2014) 1345 – 1358, ISSN 1433-3015, doi:10.1007/s00170-013-5594-5.

[10] B. Yilbas, S. Akhtar, O. Keles, Laser cutting of triangular blanks from thick aluminum foam plate: Thermal stress analysis and morphology, Appl. Therm. Eng. 62 (1) (2014) 28 – 36, ISSN 1359-4311, doi:10.1016/j.applthermaleng.2013.09.026.

[11] I. Roberts, C. Wang, R. Esterlein, M. Stanford, D. Mynors, A three-dimensional finite element analysis of the temperature field during laser melting of metal powders in additive layer manufacturing, Int. J. Mach. Tool. Manu. 49 (12-13) (2009) 916 – 923, ISSN 0890-6955, doi:10.1016/j.ijmachtools.2009.07.004.

[12] R. Akarapu, B. Li, A. Segall, A thermal stress and failure model for laser cutting and forming operations, Journal of Failure Analysis and Prevention 4 (5) (2004) 51 – 62, ISSN 1864-1245, doi:10.1361/15477020420756.

[13] K. Nyon, C. Nyeoh, M. Mokhtar, R. Abdul-Rahman, Finite element analysis of laser inert gas cutting on Inconel 718, Int. J. Adv. Manuf. Tech. 60 (9) (2011) 995 – 1007, ISSN 1433-3015, doi:10.1007/s00170-011-3655-1.

[14] C. Fu, M. Sealy, Y. Guo, X. Wei, Finite element simulation and experimental validation of pulsed laser cutting of nitinol, Journal of Manufacturing Processes 19 (2015) 81 – 86, ISSN 1526-6125, doi:10.1016/j.jmapro.2015.06.005.

[15] M. Modest, Three-dimensional, Transient model for laser machining of ablating/decomposing materials, Int. J. Heat Mass Trans. 39 (2) (1996) 221 – 234, ISSN 0017-9310, doi:10.1016/0017-9310(95)00134-U.

[16] M. Modest, Laser through-cutting and drilling models for ablating/decomposing materials, J. Laser Appl. 9 (3) (1997) 137 – 145, doi:10.2351/1.4745453.

[17] G. Han, S. Na, A study on torch path planning in laser cutting processes part 1: Calculation of heat flow in contour laser beam cutting, J. Manuf. Syst. 18 (2) (1999) 54 – 61, ISSN 0278-6125, doi:10.1016/S0278-6125(99)80026-0.

[18] W. Xu, J. Fang, X. Wang, T. Wang, F. Liu, Z. Zhao, A numerical simulation of temperature field in plasma-arc forming of sheet metal, J. Mater. Process. Tech. 164 - 165 (2005) 1644 – 1649, ISSN 0924-0136, doi:10.1016/j.jmatprotec.2005.01.007.

[19] M. Kim, Transient evaporative laser-cutting with boundary element method, Appl. Math. Model. 25 (1) (2000) 25 – 39, ISSN 0307-904X, doi:10.1016/S0307-904X(00)00034-2.

[20] M. Kim, Transient evaporative laser cutting with moving laser by boundary element method, Appl. Math. Model. 28 (10) (2004) 891 – 910, ISSN 0307-904X, doi:10.1016/j.apm.2004.03.001.

[21] K. Kheloufi, A. Hachemi, A. Benzaoui, Numerical simulation of Transient three-dimensional temperature and kerf formation in laser fusion cutting, J. Heat Trans. - T. ASME 137 (11), ISSN 112101-112101-9, doi:10.1115/1.4030658.

[22] P. Yuan, D. Gu, Molten pool behaviour and its physical mechanism during selective laser melting of TiC/AlSi10Mg nanocomposites: simulation and experiments, J. Phys. D. - Appl. Phys. 48 (3) (2015) 035303.

[23] M. S. Gross, On gas dynamic effects in the modelling of laser cutting processes, Appl. Math. Model. 30 (4) (2006) 307 – 318, ISSN 0307-904X, doi:10.1016/j.apm.2005.03.021.

[24] H. Boffy, M. Baietto, P. Sainsot, A. Lubrecht, Detailed modelling of a moving heat source using multigrid methods, Tribol. Int. 46 (1) (2012) 279 – 287, ISSN 0301-679X, doi:10.1016/j.triboint.2011.06.011.

[25] N. Gupta, N. Nataraj, A posteriori error estimates for an optimal control problem of laser surface hardening of steel, Adv. Comput. Math. 39 (1) (2013) 69 – 99, ISSN 1572-9044, doi:10.1007/s10444-011-9270-8.

[26] M. Modest, H. Abakians, Evaporative Cutting of a Semi-infinite Body With a Moving CW laser, J. Heat Trans. - T. ASME 108 (3) (1986) 602 – 607, doi:10.1115/1.3246978.

[27] K. Zimmer, Analytical solution of the laser-induced temperature distribution across internal material interfaces, Int. J. Heat

Mass Trans. 52 (1-2) (2009) 497 – 503, ISSN 0017-9310, doi: 10.1016/j.ijheatmassTransfer.2008.03.034.

[28] S. Mullick, Y. Madhukar, S. Roy, A. Nath, An investigation of energy loss mechanisms in water-jet assisted underwater laser cutting process using an analytical model, Int. J. Mach. Tool. Manu. 91 (2015) 62 – 75, ISSN 0890-6955, doi:10.1016/j.ijmachtools.2015.02.005.

[29] S. Mullick, Y. Madhukar, S. Roy, A. Nath, Performance optimization of water-jet assisted underwater laser cutting of AISI 304 stainless steel sheet, Opt. Laser Eng. 83 (2016) 32 – 47, ISSN 0143-8166, doi:10.1016/j.optlaseng.2016.02.022.

[30] H.-J. Jiang, H.-L. Dai, Effect of laser processing on three dimensional thermodynamic analysis for HSLA rectangular steel plates, Int. J. Heat Mass Trans. 82 (2015) 98 – 108, ISSN 0017-9310, doi: 10.1016/j.ijheatmassTransfer.2014.11.003.

[31] J. Winczek, Analytical solution to Transient temperature field in a half-infinite body caused by moving volumetric heat source, Int. J. Heat Mass Trans. 53 (25-26) (2010) 5774 – 5781, ISSN 0017-9310, doi: 10.1016/j.ijheatmassTransfer.2010.07.065.

[32] P. Parandoush, A. Hossain, A review of modeling and simulation of laser beam machining, Int. J. Mach. Tool. Manu. 85 (2014) 135 – 145, ISSN 0890-6955, doi:10.1016/j.ijmachtools.2014.05.008.

[33] P. D. Pietro, Y. Yao, A numerical investigation into cutting front mobility in C02 laser cutting, Int. J. Mach. Tool. Manu. 35 (5) (1995) 673 – 688, ISSN 0890-6955, doi:10.1016/0890-6955(95)93037-7.

Appendix

The analytic solution to Eq. (8) for a linear trajectory $\mathbf{x}_0(t) = \mathbf{v}t + \mathbf{p}$ ($\mathbf{v} = [v_x, v_y]$ and $\mathbf{p} = [p_x, p_y]$) is presented here for a point source (Dirac delta) laser beam and a square-shape laser beam.

Dirac Delta Laser Coefficients

$$\begin{aligned}
&\int_{t_0}^{t}\int_0^b\int_0^a f_{Dirac}(\mathbf{x},\mathbf{x}_0)\mathbb{X}_i(x)\mathbb{Y}_j(y)e^{-\omega_{ij}(t-\tau)}dxdyd\tau \\
&\quad = P(1-R)\int_{t_0}^{t} e^{-\omega_{ij}(t-\tau)}\sin\frac{i\pi x_0(\tau)}{a}\sin\frac{j\pi y_0(\tau)}{b}d\tau \\
&\quad = P(1-R) \\
&\quad \Big[\sin\beta_x\sin\beta_y\int_0^{t-t_0} e^{-\omega_{ij}((t-t_0)-\tau)}\cos\alpha_x\tau\cos\alpha_y\tau d\tau \\
&\quad + \sin\beta_x\cos\beta_y\int_0^{t-t_0} e^{-\omega_{ij}((t-t_0)-\tau)}\cos\alpha_x\tau\sin\alpha_y\tau d\tau \\
&\quad + \cos\beta_x\sin\beta_y\int_0^{t-t_0} e^{-\omega_{ij}((t-t_0)-\tau)}\sin\alpha_x\tau\cos\alpha_y\tau d\tau \\
&\quad + \cos\beta_x\cos\beta_y\int_0^{t-t_0} e^{-\omega_{ij}((t-t_0)-\tau)}\sin\alpha_x\tau\sin\alpha_y\tau d\tau\Big]
\end{aligned} \tag{.1}$$

Square-Shape Laser Coefficients

$$\begin{aligned}
&\int_{t_0}^{t}\int_0^b\int_0^a f_{square}(\mathbf{x},\mathbf{x}_0)\mathbb{X}_i(x)\mathbb{Y}_j(y)e^{-\omega_{ij}(t-\tau)}dxdyd\tau \\
&\quad = \frac{P(1-R)}{\Delta x^2}\int_{t_0}^{t} e^{-\omega_{ij}((t-t_0)-\tau)} \\
&\quad \left(\int_{x_0(\tau)-\frac{\Delta x}{2}}^{x_0(\tau)+\frac{\Delta x}{2}}\sin\frac{i\pi x}{a}dx\right)\left(\int_{y_0(\tau)-\frac{\Delta x}{2}}^{y_0(\tau)+\frac{\Delta x}{2}}\sin\frac{j\pi y}{b}dy\right)d\tau \\
&\quad = \frac{abP(1-R)}{ij\pi^2\Delta x^2} \\
&\quad \Big[c_1c_3\int_0^{t-t_0} e^{-\omega_{ij}((t-t_0)-\tau)}\cos\alpha_x\tau\cos\alpha_y\tau d\tau \\
&\quad - c_1c_4\int_0^{t-t_0} e^{-\omega_{ij}((t-t_0)-\tau)}\cos\alpha_x\tau\sin\alpha_y\tau d\tau \\
&\quad - c_2c_3\int_0^{t-t_0} e^{-\omega_{ij}((t-t_0)-\tau)}\sin\alpha_x\tau\cos\alpha_y\tau d\tau \\
&\quad + c_2c_4\int_0^{t-t_0} e^{-\omega_{ij}((t-t_0)-\tau)}\sin\alpha_x\tau\sin\alpha_y\tau d\tau\Big]
\end{aligned} \tag{.2}$$

Where:

$$
\begin{aligned}
c_1 = \cos\beta_x - \cos\gamma_x, &\quad c_2 = \sin\beta_x - \sin\gamma_x, \\
c_3 = \cos\beta_y - \cos\gamma_y, &\quad c_4 = \sin\beta_y - \sin\gamma_y, \\
\alpha_x = \frac{i\pi v_x}{a}, &\quad \alpha_y = \frac{j\pi v_y}{b}, \\
\beta_x = \frac{i\pi(p_x + \Delta x/2)}{a}, &\quad \beta_y = \frac{j\pi(p_y + \Delta x/2)}{b}, \\
\gamma_x = \frac{i\pi(p_x - \Delta x/2)}{a}, &\quad \gamma_y = \frac{j\pi(p_y - \Delta x/2)}{b}
\end{aligned}
\tag{.3}
$$

$$
\begin{aligned}
&\int_0^t e^{-\omega(t-\tau)} \cos\alpha\tau \cos\beta\tau d\tau \\
&\quad = C\left[\alpha^3 \sin\alpha t \cos\beta t + \beta^3 \cos\alpha t \sin\beta t + \omega^3 \cos\alpha t \cos\beta t\right. \\
&\quad - \alpha^2\beta \cos\alpha t \sin\beta t + \alpha^2\omega \cos\alpha t \cos\beta t - \alpha\beta^2 \sin\alpha t \cos\beta t \\
&\quad + \beta^2\omega \cos\alpha t \cos\beta t + \alpha\omega^2 \sin\alpha t \cos\beta t + \beta\omega^2 \cos\alpha t \sin\beta t \\
&\quad \left.+2\alpha\beta\omega \sin\alpha t \sin\beta t - \omega e^{-\omega t}(\alpha^2 + \beta^2 + \omega^2)\right]
\end{aligned}
\tag{.4}
$$

$$
\begin{aligned}
&\int_0^t e^{-\omega(t-\tau)} \sin\alpha\tau \sin\beta\tau d\tau \\
&\quad = -C\left[\alpha^3 \cos\alpha t \sin\beta t + \beta^3 \sin\alpha t \cos\beta t - \omega^3 \sin\alpha t \sin\beta t\right. \\
&\quad - \alpha^2\beta \sin\alpha t \cos\beta t - \alpha^2\omega \sin\alpha t \sin\beta t - \alpha\beta^2 \cos\alpha t \sin\beta t \\
&\quad - \beta^2\omega \sin\alpha t \sin\beta t + \alpha\omega^2 \cos\alpha t \sin\beta t + \beta\omega^2 \sin\alpha t \cos\beta t \\
&\quad \left.-2\alpha\beta\omega(\cos\alpha t \cos\beta t - e^{-\omega t})\right]
\end{aligned}
\tag{.5}
$$

$$
\begin{aligned}
&\int_0^t e^{-\omega(t-\tau)} \cos\alpha\tau \sin\beta\tau d\tau \\
&\quad = C\left[\alpha^3 \sin\alpha t \sin\beta t - \beta^3 \cos\alpha t \cos\beta t + \omega^3 \cos\alpha t \sin\beta t\right. \\
&\quad + \alpha^2\beta \cos\alpha t \cos\beta t + \alpha^2\omega \cos\alpha t \sin\beta t - \alpha\beta^2 \sin\alpha t \sin\beta t \\
&\quad + \beta^2\omega \cos\alpha t \sin\beta t + \alpha\omega^2 \sin\alpha t \sin\beta t - \beta\omega^2 \cos\alpha t \cos\beta t \\
&\quad \left.-2\alpha\beta\omega \sin\alpha t \cos\beta t - \beta e^{-\omega t}(\alpha^2 - \beta^2 - \omega^2)\right]
\end{aligned}
\tag{.6}
$$

$$
C = \frac{1}{\alpha^4 + \beta^4 + \omega^4 - 2\alpha^2\beta^2 + 2\alpha^2\omega^2 + 2\beta^2\omega^2}
\tag{.7}
$$

LaTeX Source Files
Click here to download LaTeX Source Files: Main.rar